Digital holographic microscopy investigation of second harmonic generated at a glass/air interface

Etienne Shaffer,* Nicolas Pavillon, Jonas Kühn, and Christian Depeursinge

École Polytechnique Fédérale de Lausanne (EPFL), Advanced Photonics Laboratory, 1015 Lausanne, Switzerland
*Corresponding author: etienne.shaffer@epfl.ch

Optical second-harmonic generation, thanks to its coherent nature, is a suitable signal for interferometric measurements such as digital holography, a well-established imaging technique that allows recovery of complex diffraction wave fields from which it is possible to extract both amplitude-contrast and quantitative phase images. Here, we report on a multifunctional form of microscopy, namely, second-harmonic generation digital holographic microscopy. As a proof of concept, we have investigated the second-harmonic signal generated at the glass/air interface of a microscope slide under focused femtosecond laser illumination, and we propose, for the first time to our knowledge, a representation and interpretation of the recovered phase. In this simple yet educative case study, we observe that the second harmonic is generated by the axial component of the incident field polarization. © 2009 Optical Society of America

OCIS codes: 090.1995, 180.4315.

Over the past decades, nonlinear light–matter interactions have proven very useful in microscopy. To mention only one, harmonic generation allows marker-free identification of cell structures, tubulin, or membranes [1], while being extremely sensitive to the local sample structure and to the orientation of the laser polarization [2]. It has even been demonstrated that membrane potentials of labeled neurons could be monitored by observation of the second-harmonic generation (SHG) signal [3]. On the other hand, digital holographic microscopy (DHM) performs well for both metrology and biological applications, since it can reveal deformations and morphological details at a nanometer-scale resolution [4] and can determine with high precision the refractive index distribution across a specimen [5] (e.g., cell or neuron). Apart from being a nonintrusive, nondestructive real-time imaging technique, DHM is also versatile, and its principle can be applied to any coherent optical field, including those generated by some nonlinear light–matter interactions.

In this Letter, we propose to combine SHG with DHM in order to take advantage of the additional information provided by the phase of the second harmonic signal. This Letter distinguishes from previous pioneer work on coherent SHG imaging [6,7] by recovering, for the first time to our knowledge, the complex (amplitude and phase) harmonic field, while [6] investigated signal-to-noise ratio enhancement from interferometric measurement of harmonic fields, and [7] proposed novel nanoparticle markers, called second harmonic radiation imaging probes (SHRIMPs), for second-harmonic imaging.

In digital holography, interference patterns (holograms) are recorded by a digital camera. In opposition to the classical holography, no photochemical development step is required, and the image reconstruction is performed numerically. In our configuration, the detector is located at a certain distance from the system image plane, and the intensity I_H recorded at the hologram plane is the resulting interference of the object wave **O** with one reference wave **R** and can be expressed as

$$I_H(x,y) = \mathbf{OO}^* + \mathbf{RR}^* + \mathbf{OR}^* + \mathbf{RO}^*, \qquad (1)$$

where the first two terms form a zero-order of diffraction and the last two, respectively, correspond to the real and the virtual images. The star symbol (*) denotes the complex conjugate. Working in an off-axis configuration, i.e., giving a nonzero angle of incidence between the object and reference waves, allows for Fourier filtering of a spatial frequency-modulated image term from all other terms in Eq. (1) [8]. However, the angle between the two waves must be kept small enough that the fringes are appropriately sampled by the detector. More information on the application of Fourier filtering to our off-axis holographic technique can be found in [9]. After Fourier filtering out the zero-order of diffraction and the conjugate image, the complex wave is digitally focused by means of a single Fresnel propagation, as explained in detail in [10]. Optical aberrations can be compensated by the application of numerical parametric lenses to the complex wave front, either or both in the hologram plane and/or the image plane [11].

Schematics of the optical setup used for experiments can be found in Fig. 1. The laser source is a Mira Ti:sapphire femtosecond laser from Coherent, equipped with a RegA9000 regenerative amplifier stage delivering 800 nm wavelength, 250 fs pulses at approximately 250 kHz. The interferometric setup consists mainly of one object arm containing the specimen and one reference arm. In the object arm, light is focused in the specimen plane by a lens with a relative aperture ($f/\#$) of 0.8 and then collected by a $100\times$ microscope objective. A frequency doubler β-barium borate crystal is inserted in the reference arm to generate the second-harmonic reference wave. Holograms were recorded using a $-20\,°$C-cooled
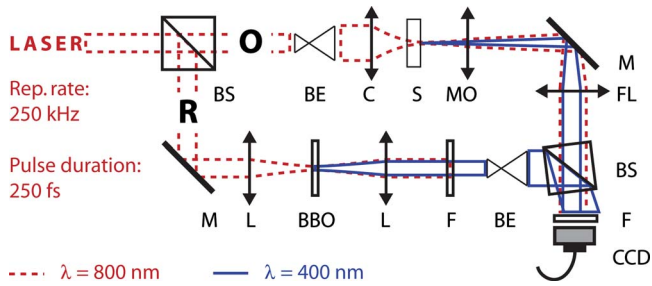
Fig. 1. (Color online) Experimental setup schematics: BS, beam splitter; BE, beam expander with pinhole-based spatial filtering; C, condenser lens; S, specimen; MO, microscope objective; M, mirror; FL, field lens; F, wavelength-selective filter; L, lens; BBO, frequency doubler β-barium borate crystal.

Hamamatsu Orca-ER CCD camera, and a 400 ± 20 nm bandpass filter was used to get rid of the fundamental-wavelength component of light. The laser peak power in the specimen plane is approximately 30 GW cm^{-2} pulse^{-1}, which is about 1 order of magnitude below the threshold for biological cell damage [12], and could potentially be reduced by use of a more sensitive camera, e.g., an electron-multiplying CCD type. The lateral resolution of this technique is diffraction limited at the SHG wavelength (here, 400 nm), and the axial resolution can reach the nanometer scale, thanks to its interferometric nature. The specimen investigated in the experiments described in this Letter was a glass microscope slide.

Experimentally, we have recorded a hologram of the second-harmonic signal generated at the second interface of a microscope slide, where a linearly x-polarized, fundamental-wavelength laser beam was focused (Fig. 2). We assume the second harmonic signal generated at the first interface to be negligible, since the glass slide is relatively thick (1 mm) and, in our configuration, the incident field converges rapidly. Both amplitude [Fig. 3(a)] and phase [Fig. 3(b)] images have been reconstructed. We have observed that the symmetric, dipole-like pattern of the retrieved second harmonic signal maps is related to the polarization state of the incident field. Because SHG is a second-order nonlinear optical phenomenon, Fig. 3(a) maps the square value of the electric field distribution that contributed to SHG, and the latter obviously differs from the expected total electric field of a focused Gaussian field.
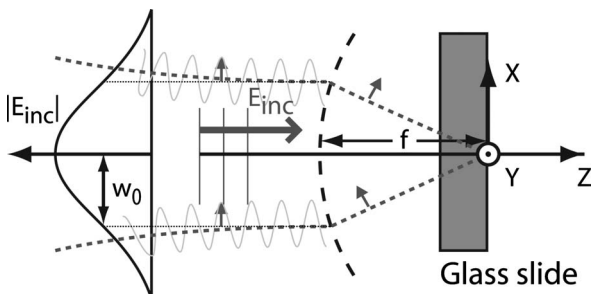

Fig. 2. The x-polarized Gaussian field $\mathbf{E}_{\text{inc}}$ of waist w_0 is focused by a lens of relative aperture $f/\# = f/2w_0$ on the second interface of a glass slide.
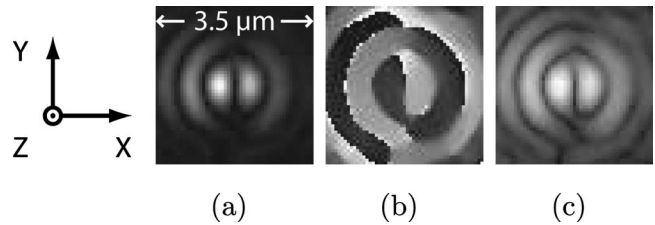

Fig. 3. (a) Experimental amplitude and (b) relative phase of the optical second-harmonic signal generated at the interface, as retrieved by digital holographic microscopy. (c) Square root of the experimental SHG amplitude for direct comparison with incident, fundamental field amplitude of Fig. 4(c).

To provide a better understanding of the retrieved SHG images, we have modeled the electric field distribution of a focused Gaussian laser beam, using the theory established by Richards and Wolf [13,14], as described in [15]. This method calculates the complex field in the focal plane ($z = 0$) by taking into account the angular spectrum contribution of all light rays refracted by a condenser lens of a given aperture (here, $f/0.8$). We considered a linearly x-polarized Gaussian field, whose waist is located in the plane of the condenser lens that focuses it on the second face of a microscope slide, as depicted in Fig. 2. As we are interested only in the relative light intensity at the interface where the second harmonic is generated, we have neglected prior reflections and have assumed perfect transmission coefficients at the interface. Figure 4 shows the calculated amplitude and phase of the x, y, and z-polarized Cartesian components of the focused field. The conversion of the x-polarization state into x-, y-, and z-polarization states under focusing of the field by a lens is known as depolarization and is detailed in [16] on the complex three-dimensional (3D) amplitude point-spread function.

As with any second-order nonlinear optical phenomenon, SHG can occur only in noncentrosymmetric media or at interfaces, where the symmetry is obviously broken. In our case, this symmetry break lies
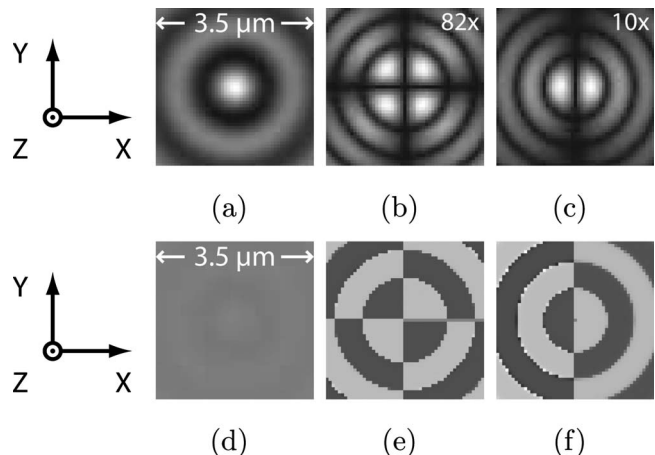

Fig. 4. Respectively displayed in (a), (b), and (c) are the amplitudes of the x-, y-, and z-polarized components in the focal plane of a linearly x-polarized Gaussian field focused by a $f/0.8$ lens, in air. Amplitudes in (b) and (c) have been respectively scaled by $82\times$ and $10\times$. The corresponding phases are displayed in (d), (e), and (f).

in the axial z direction, where the medium abruptly changes from glass to air. Therefore, only the z component of the incident field should effectively contribute to the SHG, which is what a comparison between the experimental SHG images and the calculated z-component distribution of the incident field reveals. The matching phase images [Figs. 3(b) and 4(f)] especially emphasize the coherent nature of SHG. As for the amplitude images, it must be remembered that the second-harmonic wave field is proportional to the square of the electric field. Therefore the electric field amplitude image in Fig. 4(c) has to be compared to the square root of the SHG amplitude image, as presented in Fig. 3(c), in which case the correspondence is very good. It is worth noting that since the second harmonic is generated by the z component of the electric field, its intensity strongly depends on the relative aperture of the condenser lens.

In conclusion, we have successfully recorded second-harmonic wavelength holograms, extracted the complex field, and reconstructed both amplitude and quantitative phase images, which is, to our knowledge, unprecedented. While the phase signal in conventional DHM carries information on the optical path length that is perceived by the photons, the harmonic phase provides additional, quantitative information about the relative phase of the surface dipoles where the second harmonic is generated, which we have used to identify the polarization component responsible for SHG at the glass/air interface. Because it recovers the complex wave field, the technique also makes possible the determination of the precise location where the second harmonic is generated and could potentially serve as a tool to map 3D distribution of SHG-emitting nanoparticles, such as gold nanoparticles. On a more general note, we believe that the phase information provided by this technique may become a key element in functional, nonlinear imaging.

References

1. W. R. Zipfel, R. M. Williams, R. Christie, A. Y. Nikitin, B. T. Hyman, and W. W. Webb, Proc. Natl. Acad. Sci. USA **100**, 7075 (2003).
2. S. W. Chu, S. Y. Chen, G. W. Chern, T. H. Tsai, Y. C. Chen, B. L. Lin, and C. K. Sun, Biophys. J. **86**, 3914 (2004).
3. D. A. Dombeck, M. Blanchard-Desce, and W. W. Webb, J. Neurosci. **24**, 999 (2004).
4. J. Kühn, F. Charrière, T. Colomb, E. Cuche, F. Montfort, Y. Emery, P. Marquet, and C. Depeursinge, Meas. Sci. Technol. **19**, 1 (2008).
5. P. Marquet, B. Rappaz, P. J. Magistretti, E. Cuche, Y. Emery, T. Colomb, and C. Depeursinge, Opt. Lett. **30**, 468 (2005).
6. Y. Pu, M. Centurion, and D. Psaltis, Appl. Opt. **47**, A103 (2008).
7. C.-L. Hsieh, R. Grange, Y. Pu, and D. Psaltis, Opt. Express **17**, 2880 (2009).
8. E. N. Leith and J. Upatnieks, J. Opt. Soc. Am. **52**, 1123 (1962).
9. E. Cuche, P. Marquet, and C. Depeursinge, Appl. Opt. **39**, 4070 (2000).
10. U. Schnars and W. P. O. Juptner, Meas. Sci. Technol. **13**, R85 (2002).
11. T. Colomb, F. Montfort, J. Kühn, N. Aspert, E. Cuche, A. Marian, F. Charrière, S. Bourquin, P. Marquet, and C. Depeursinge, J. Opt. Soc. Am. A **23**, 3177 (2006).
12. K. König, P. T. C. So, W. W. Mantulin, and E. Gratton, Opt. Lett. **22**, 135 (1997).
13. E. Wolf, Proc. R. Soc. London Ser. A **253**, 349 (1959).
14. B. Richards and E. Wolf, Proc. R. Soc. London Ser. A **253**, 358 (1959).
15. L. Novotny and B. Hecht, *Principles of Nano-Optics* (Cambridge U. Press, 2006).
16. A. Marian, F. Charrière, T. Colomb, F. Montfort, J. Kühn, P. Marquet, and C. Depeursinge, J. Microsc. **225**, 156 (2007).